Design and durability study of environmental-friendly room-temperature processable icephobic coatings

Wu, Xinghua; Zhao, Xin; Ho, Jeffrey Weng Chye; Chen, Zhong

2018

Wu, X., Zhao, X., Ho, J. W. C., & Chen, Z. (2019). Design and durability study of environmental-friendly room-temperature processable icephobic coatings. Chemical Engineering Journal, 355, 901-909. doi:10.1016/j.cej.2018.07.204

https://hdl.handle.net/10356/143557

https://doi.org/10.1016/j.cej.2018.07.204

Design and Durability Study of Environmental-friendly Room-Temperature Processable Icephobic Coatings

Xinghua Wu, Xin Zhao, Jeffrey Weng Chye Ho, Zhong Chen*

School of Materials Science and Engineering, Nanyang Technological University, 50 Nanyang Avenue, 639798, Singapore

Abstract: Ice accumulation leads to improper functioning or even damages to ships, offshore platforms, sports facilities and land buildings in cold climate regions. Although fluorochemicals have demonstrated attractive performance for icephobic applications, their use has been restricted due to health and environmental concerns. Here, we present a facile method to fabricate fluorine-free icephobic coatings with potential applications for outdoor facilities and structures. The coating consists of a silicone-epoxy hybrid resin, polydimethylsiloxane (PDMS) and SiO_2 nanoparticles with different sizes. Particularly, the use of different sized (10-20 nm and 200 nm) SiO_2 nanoparticles results in excellent icephobicity and mechanical properties. The mechanical properties and durability of the coating were analysed according to respective test standards and compared with reported icephobic coatings. The durable icephobic potency of the coatings is very promising as a sustainable green solution for various practical anti-icing applications.

1

PDMS, polydimethylsiloxane; UV, ultraviolet; NPs, nanoparticles; GFRE, glass fibers reinforced epoxy; PU, polyurethane; CSM, continuous stiffness measurement; DI, deionized; SLIPs, slippery liquid infused surfaces; SLIC, self-lubricating icephobic elastomer coating.

1. Introduction

To reduce the labour cost and downtime associated with removal of accumulated ice on facilities, transportation vehicles, and buildings, considerable interest on anti-icing coatings has been shown since the 1900s. The first reported anti-icing composition designed for automobile radiator was patented in 1918.[1] In 1956, Rolle and Barnes claimed that cellulose lacquers could withstand the icing and de-icing test.[2] Jellinek studied the effect of a monolayer on ice adhesion in 1962.[3] Bascom et al. investigated the ice-adhesion strength of hydrophobic and hydrophilic surfaces, and the failure mechanism of hydrophilic surfaces.[4] Since then, a lot of research work has been carried out, ranging from liquid & grease filled coatings to modified epoxy or urethane paints.[5, 6] Literature study shows that the adhesion strength between ice and solid surfaces depends greatly on the van der Waals forces.[7] In recent years, there has been a growing interest in superhydrophobic coatings consisting of hierarchical micro-nano structures.[8-11] The trapped air pockets on such coating surface are beneficial in reducing the adhesion of ice as they are able to decrease the actual contact area. In addition, the presence of air between ice and the coating surface reduces heat transfer, and at the same time provides stress loci to initiate cracks between the substrate and ice during ice removal.[7, 12] However, the existing of micro-nano structures weakens the mechanical durability of superhydrophobic coatings, and in some cases, moisture condensation in the micro / nanoporous surface may lead to a larger (than the nominal) contact area between ice and the solid surface, resulting in an increased ice adhesion.

Slippery liquid-infused porous surfaces (SLIPs), inspired by *Nepenthes* pitcher plants, have been explored by some researchers as another strategy to achieve low ice adhesion.[13] Liu et al. prepared anti-icing SLIPs coatings from silicone rubber solution.[14] Zhang et al. reported a

double-layered SLIPs coating prepared by hydrothermal reaction followed with perfluoropolyether liquid infusion.[15] An ice releasing coating was manufactured by silicone oil or fluorosilicone fluid embedded within cross-linked silicone resin.[16] The major challenges faced by SLIPs are the potential depletion of infused liquids and poor mechanical properties of the porous matrix. Yeong et al. developed an oil-infused icephobic elastomeric coating (SLIC) which showed good durability to abrasion by self-replenishing the lost oil.[17] In another effort to avoid depletion of the infused liquid, Coady et al. infused UV-cured siloxane resin into anodized coupons treated with *n*-decyltrichlorosilane and silicone oil.[18] However, after seven de-icing cycles, removal of resin/oil layer was observed.

Among existing reports, epoxy coatings are practically favourable with the advantage of low cost, no limitation on the dimension and shape of targeted substrates, being scalable and easy to process at low temperatures. Li et al. reported a fluorinated coating embedded with surface-modified nano-silica which is promising for anti-icing applications.[19] The coating exhibits superhydrophobicity after 4 weeks of acid / alkali, heat / cool treatment. Atta et al. successfully prepared superhydrophobic epoxy coatings with the help of fatty acids modified calcium carbonate nanoparticles.[20] Moreover, magnetic nanoparticles which could be used as heat mediators were introduced into fluorinated epoxy resin by Zhang et al., and they obtained superhydrophobic coating exhibited ice-adhesion strength around 200 kPa.[21] Guo's group demonstrated anti-icing coatings fabricated by spreading $Mg(OH)_2$ particles treated with stearic acid on top of epoxy resins.[22] Despite these advances, work focusing on the mechanical properties and durability of icephobic coatings remains limited, especially anti-icing properties under ultraviolet (UV) irradiation and harsh sand erosion environment. Considering that there are different requirements for the mechanical properties and durability for different practical

3

applications (e.g. aeroplane wings vs. wind turbine blades), icephobic materials that can display good resistance to ice formation and accumulation under different application environments are highly desirable.

In terms of the low surface energy materials, fluorocarbons are often used in icephobic coatings. For example, Zhang et al. demonstrated a slippery anti-icing coating by trapping perfluoropolyether in the porous AZ31 Mg alloy.[15] Emelyanenko et al. fabricated a fluorooxysilane modified silicone rubber coating with the help of laser treatment, and investigated the anti-icing behavior at low temperatures.[23] However, fluorochemicals are bio-accumulative and potentially harmful to human health. Industries have started to ban the use of long-chain fluorocarbons. As a result, research activity has been in the rise to seek effective replacement for fluorochemicals in hydrophobic and icephobic coatings. In this paper, we fabricated fluorine-free superhydrophobic coatings via a facile method based on silicone-epoxy resin and dual-scale SiO_2 nanoparticles design. The process is simple, and the coating can be cured at room temperature. The prepared coatings were tested under simulated harsh environments such as pressurized sand erosion and UV / condensation exposure. The developed superhydrophobic coatings demonstrated excellent durability, and are promising for practical applications.

2. Experimental details

2.1. Materials

SiO_2 nanoparticles (NPs) with sizes of 10-20 nm and 200 nm, and butyl acetate (99 wt. %) were obtained from Sigma Aldrich. A commercially available silicone-epoxy hybrid resin (SILIKOPON® EF) and polydimethylsiloxane (PDMS, commercial name Sylgard 184) were

obtained from Evonik industries and Dow Corning, respectively. Both are two-part products and were used with weight ratio between the base and hardener at 2 : 1 and 10 : 1, respectively. Tinuvin 292, obtained from BASF, was used as UV stabilizer. Substrates were cut from glass fibers reinforced epoxy (GFRE) plates. For comparison, proprietary polyurethane based composite coating, formulated for wind turbine applications (denoted as the PU coating thereafter), was acquired and tested.

2.2. Preparation method

In a typical fabrication process, PDMS grafted SiO_2 NPs was prepared by mixing the elastomer base, its curing agent, and butyl acetate as the solvent for 10 min. The weight ratio of base : curing agent : solvent : silica particles was 1 : 0.1 : 20 : 4. To investigate the effect of dual-sized SiO_2 NPs, comparison was made between the PDMS modified two sized particles (200 nm and 10-20 nm with weight ratio of 1 : 2 mixed) and the 10-20 nm particles only. SILIKOPON® EF (two parts used together) and Tinuvin 292 were added into the prepared SiO_2 particle suspensions and mixed for another 10 min under ambient condition. The detailed weight ratio of the mixtures and sample ID are show in Table 1. S20 denotes the coating containing the single-sized 10-20 nm particles, while S200 stands for the coating containing the dual sized silica particles (200 nm and 10-20 nm). A mechanical mixer was used during the mixing process at a speed of 2000 rpm. The obtained particle dispersion solutions were spray-coated onto the GFRE substrates through an airbrush kit (AS06KB) with a 1.5 mm diameter nozzle using compressed air (pressure at 345 kPa). The distance between the airbrush and the substrate was kept at 10 cm. The airbrush was moved laterally back and forth until a uniform coating has been deposited. After 24 h curing at room temperature, superhydrophobic coatings were obtained.

2.3. Characterization and mechanical testing

The surface morphology of the coatings was observed using a field emission scanning electron microscope (FESEM, JEOL-7600F, Japan). The contact angle and roll-off angle of water were measured with a contact angle system (OCA 20, Dataphysics Co., Germany). The surface roughness of the coatings was evaluated by a surface profiler (Alpha-Step IQ Surface Profiler, Kla Tencor, USA) with a scanning length of 6 mm. FTIR spectra of the coatings were obtained using a Frontier™ IR/FIR spectrometer (Perkin-Elmer Inc.). The tested samples were prepared by mixing the coating fragments and standard KBr powders with weight ratio of 1:20, followed by compression. The coatings fragments were scratched from the coatings. The elastic modulus and hardness of the deposited coatings were measured using a nano-indenter (Nano Indenter XP® system, MTS, US) with continuous stiffness measurement (CSM) method.[24] 10 ~ 12 indents were made on each sample. At least three samples of each type of coating were tested. Considering the effect of surface roughness, averaged results were obtained in the depth range of 1500 ~ 2000 nm. For the PU coating, because of its elastomeric nature, continuous stiffness measurement may not be appropriate. Therefore, static loading was used for PU coating. The hardness and Young's modulus values were obtained at the same depth range, 1500 ~ 2000 nm, as in the CSM method. Pencil scratch test of coatings was assessed using a commercial pencil-scratch tester (Scratch Hardness Tester Model 291, ERICHSEN, Germany) according to ISO 15184 standard test method. The brittleness and adhesion properties of coatings were measured by a cross-cut adhesion test kit (Cross Cut Adhesion Test KIT CC1000, TQC, Netherlands) based on ISO 2409 standard test method. After the cross cutting, the surfaces were examined under optical microscope (Olympus BX51, Japan). The bond strength between

coatings and GFRE substrates was conducted by an adhesion tester (PosiTest AT-M20, Defescal, USA) according to ISO 4624 standard.

2.4. Durability assessment

UV resistance of the coatings was analyzed by a UV accelerated weathering machine (SDL ATLAS, UK) according to ISO 11507 standard. Samples were mounted in the weathering chamber and subjected to a cycle of 4 hours exposure to intense UV radiation at 60 °C, followed by 4 hours moisture exposure by condensation at 50 °C. The cycle was continued for a total of 288 hours. In addition, a home designed micro-sand blaster was also used to investigate the anti-icing durability of coatings after sand erosion.[25] Silica particles in size of 63 μm (220 mesh) were used as the erosion media. The coatings were placed horizontally under the sand spraying nozzle with a distance of 10 cm. The erosion was carried out by impinging the sand particles perpendicular onto the coating surface for 30 s at a pressure of 200 kPa over an exposed area of 2.43 cm^2. The loss in weight was recorded after the sand erosion test. Optical microscope and FESEM were used to observe the eroded regions on the coating surface. Change in water wettability and icephobicity of the coatings were measured after the erosion test.

2.5. Ice-adhesion strength and ice accumulation test

To prepare for the ice-adhesion strength test, a Teflon tube with an inner diameter of 18 mm was filled with 3 ml DI water, and then covered with the coated substrate on top. The substrate was flipped upside down before being placed inside a climate chamber (Cincinnati Sub-Zero environmental chambers, USA) for 24 h at -15 °C. The prepared ice block was sheared off the substrate by a moving piston till failure.[26] The peak force at which the ice block was removed from the substrate was recorded and used for the calculation of ice-adhesion strength. The

reported ice-adhesion strength is an average value of at least six measurements on the same position of more than three samples.

Ice accumulation on the sample surface was investigated in the same climate chamber as described before at temperature of -15 °C following our previously reported method.[27] The coated substrate was placed at an angle of 45° to the horizontal plane. Pre-cooled deionized (DI) water was prepared by storing the container in a refrigerator set at -5 °C until part of the bulk water became ice (the temperature of water was therefore around 0 °C). The water dripping rate was kept at 1 drop every 5 seconds. Each ice accumulation test lasted for 10 min. The dimension of the substrate is 65 mm × 42 mm. At least three samples of each type of coatings were tested, and each sample was repeated for 3 times at the same position. The percentage accumulation with respect to the total weight of the dripped water was recorded.

3. Results and Discussion

3.1. Design Strategy

SiO_2 NPs have been widely used to prepare superhydrophobic coatings due to their cost-effectiveness, chemical durability and good mechanical properties.[28-30] Athauda et al. investigated dual-size effect of functionalized silica NPs of 7, 12, 20, and 40 nm by layer-by-layer deposition and pointed out that surface roughness can be tuned by employing NPs with different sizes.[31] Raspberry-like SiO_2 particles were prepared by some researchers to fabricate micro-nanostructure surface with superhydrophobicity.[32-34] In this study, dual-sized PDMS modified NPs (10-20 nm SiO_2 NPs and 200 nm SiO_2 NPs) were used to produce dense packing of micro-nanostructure. An in-depth and systematic study of the effect of using dual-sized

8

particles on icephobicity and mechanically durability was carried out in comparison with the single-size particles. Particularly, to enhance the mechanical durability, NPs were introduced in an epoxy matrix as shown in Figure 1a. Nanoparticles have significantly large specific surface areas and tend to agglomerate due to the van der Waals forces.[35, 36] The maximally entangled NPs offer a methodical variation of agglomeration size as well as arrangement in surface texture. Smaller NPs have larger specific surface area and greater total surface energy. When small particles are used alone, they tend to show more severe agglomeration and larger porosity as illustrated in Figure 1a. However, when the two sizes are used together, the small particles are relatively well dispersed between the large ones, effectively reducing the agglomeration and pore size as shown in the schematic illustration. For verification, single-sized and dual-sized superhydrophobic coatings were prepared. Figure 1b-c shows the obtained surface morphology of the S20 and S200 coatings, respectively. A micro-nanostructure was observed on both coating surfaces, and such surface feature is critical in introducing superhydrophobicity.[28] The micro-nanostructure enables water droplets to easily roll off the coating surface with contact angle larger than 150° as shown in Figure 1d and insets in Figure 1b-c. Between the two types of coatings, large protrusions and pores with size around 1-3 μm could be clearly seen in the S20 coatings (Figure 1b). In comparison, more densely packed surface with small pores of size less than 500 nm was observed on the S200 coatings (Figure 1c). When 33 wt.% of the 10-20 nm SiO_2 NPs were replaced by the same amount of 200 nm SiO_2 particles, a dramatic decrease in the surface porosity and protrusion size was observed. This induced a reduction in the surface roughness of coatings as shown in Figure 1e. The S20 coatings presented a surface roughness of ~1.4 μm, while the S200 exhibited a surface roughness of ~0.9 μm. Although S20 and S200

9

coatings exhibited significant difference in surface roughness values, the contact angle of S20 and S200 coatings were very close, and both are larger than 150° due to presence of the micro-nanostructure. However, S200 coatings displayed a slightly higher roll-off angle due to a lower surface roughness.

The surface chemical structure of S20 and S200 coatings is revealed by the FTIR spectra as shown in Figure 2. Since the difference of these two coatings is the size of nanoparticles, exactly the same absorption peaks were observed on these two coatings. The broad band around 3500 cm^{-1} is attributed to the OH stretching involved in absorbed water. The absorption peaks at the range of 2800 cm^{-1} ~ 3000 cm^{-1} are attributed to the C-H strength.[37-39] The absorptions peaks at 1268 cm^{-1} can be attributed to the Si-CH$_3$ group.[40] The absorptions peaks at 1081 cm^{-1}, 1095 cm^{-1}, 804 cm^{-1} and 700 cm^{-1} are related to the combined Si-O and Si–C–O stretching groups.[40, 41] The strong band at 444 cm^{-1} indicates the presence of Si-O-Si bond.[41]. No epoxy group was found at ~915 cm^{-1},[42, 43] and the small peak at 1594 cm^{-1} is attributed to the presence of NH$_2$.[44] This implies complete reaction of the epoxy resin.

3.2. Anti-icing performance

Even though the difference in surface features has limited effect on water contact angle and water roll-off angle of the S20 and S200 coatings, it may pose different impact on the icing behavior on the coatings. To better understand the anti-icing properties of S20 and S200 coatings, the commercial PU coating, which is widely used as a protective layer on outdoor facilities, were measured and compared. Figure 3a shows the measured ice-adhesion strength of PU, S20 and S200 coatings at -15 °C. The obtained ice-adhesion value for PU coatings was larger than 400 kPa and significantly higher than both S20 and S200 coatings. Besides, the

10

lowest ice-adhesion value (64.7 ± 5.4 kPa) was obtained on the S200 coatings, which was about half that of the S20 coatings. It is well accepted that the interaction forces acting at ice–substrate interface include electrostatic forces, van der Waals forces, hydrogen bonding, and mechanical interaction.[45] Although both S20 and S200 coatings contain water repellent –CH_3 groups from PDMS and silicone-epoxy hybrid resin which can better prevent or repel frost formation in the air pockets, coatings still absorb water molecules due to electrostatic forces and hydrogen bonding. Due to the high polar nature of water and ice, the directions of water molecules can be controlled by electric fields. When water freezes, the molecules still keep their polar behavior and tend to adhere to solid surface under electrostatic forces as illustrated in inset of Figure 3a (the electrostatic force is marked by the small orange dots). Coatings with larger pores allow access to a greater amount of water adsorption sites than small pores. Therefore, the S20 coating possessing larger pores provides more water absorption site than the S200 coating under high humidity and low temperature condition. Besides, larger pores in the S20 coating are prone to the sagging effect as schematically illustrated in Figure 3a (inset). This leads to greater mechanical interlocking and larger electrostatic forces between water molecular and the S20 coating surface. The less porous S200 coatings promoted and maintained the presence of tiny air pockets at the ice-coating interface. The trapped air disrupts intimate contact between the ice and the substrate, thus has significantly reduced the ice adhesion. The ice-adhesion strength of the S200 coating is much lower than the reference PU coating and some reported superhydrophobic and hydrophobic coatings which reported ice-adhesion strength larger than 400 kPa due to serious mechanical interlocking and hydrogen bonding.[45-47] The obtained adhesion strength at below 100 kPa means the ice can be easily removed by small centrifuging force, gravity, vibration or even wind

flow. Some literatures have set adhesion strength below 100 kPa as a key criterion for icephobic coatings.[48, 49]

Ice accumulation is another important criterion for icephobicity. In the current work, pre-cooled water (~0 °C) was dropwise dripped on to the PU, S20 and S200 coating surfaces at -15 °C to evaluate the resistance to ice accumulation. The obtained ice accumulation results of the three separate runs on the same position of each type of samples are shown in Figure 3**Figure 3**b. A great reduction in ice accumulation was observed on the S20 and S200 coatings compared to the PU coatings. Besides, there was no apparent difference in ice accumulation on S20 and S200 coatings due to their similar water wetting behavior. The above results are also in line with the recent experimental observations where surface wettability is a key controlling factor for reducing ice accretion and improving water drop shedding effect.[50-52] Although our coatings could not fully prevent ice accumulation, the low adhesion, particularly the one by the S200 coating, enables easy removal of the accumulated ice.

3.3. Robust mechanical properties

Mechanical properties and durability are primary concerns of anti-icing coatings for many practical applications in harsh environment. To determine the mechanical properties of S20 and S200 coatings, dolly-pull adhesion, cross-cut, pencil-scratch and nano-indentation tests were carried out according to the respective standards. The results are summarized in Table 2. Both S20 and S200 coatings demonstrated good adhesion toward the epoxy substrate according to the cross-cut test, and there were no observable coating chipping and peeling. The optical microscope images in Table 2 show that the coating edge after cutting was smoother than the reference PU coating, indicating good adhesion and non-brittleness of the coatings. The 5 %

delaminated areas of the PU coating is due to the wedge spallation failure which was caused by the applied compressive stress along the scratch groove, as well as ahead of the moving cutter.[53] The cross-cut adhesion test results of S20 and S200 coatings are comparable and are both better than currently literature reported icephobic coatings listed in Table 2.[54-58] Besides, the pencil scratch grade of 3H and 4H were obtained on the S20 and S200 coatings, respectively, which is significantly better than the PU coatings (4B) and other reported icephobic coatings.[54, 59] The dolly-pull test on S20 and S200 coatings found that the adhesion strength between coatings and substrates was stronger than that of the coatings and the applied adhesive for the test. The failure occurred at the interface of coatings and the applied adhesive as shown in Figure 4a-b. In comparison, the adhesion failure of PU coatings occurred at the interface between the substrates and PU coatings and a large peeling off area as shown in Figure 4c. Due to the different failure mechanisms, the reported pull-off data in Table 2 should not be used to compare the coating adhesion strength. The results indicate that when assessing the adhesion of hydrophobic coatings, the dolly-pull test may not be as effective as the cross-cut test despite that the former is quantitative while the latter is only quantitative. Because of the adhesive failure of S20 and S200 coatings, the actual adhesion strength of the coating to substrate should be greater that the reported value of 3.5~3.7 MPa, which is higher than the reported aeronautical livery coating [60] and silicone elastomer coating with or without intermediate layer to epoxy undercoat (adhesion strength is around 0. 431 to 1.494 MPa).[61] Further investigation was carried out to study the indentation hardness and Young's modulus of the coatings. S200 coatings presented the highest hardness and Young's modulus when compared with S20 and PU coatings. This is due to the incorporation of the nanoparticles and the reduced pore size as discussed before. Although the measured nano-indentation hardness and modulus of S200

13

coatings are lower than the reported bilayer icephobic film prepared via iCVD[62] and aeronautical livery coating,[60] pencil scratch resistance and dolly pull-off test verified the good scratch resistance and adhesion of S200 coatings to substrates.

3.4. Environmental durability

In addition to icephobicity and mechanical properties, another key requirement for a practically applicable anti-icing coating is its environmental durability under conditions such as environmental weathering and mechanical erosion. In order to simulate the UV and condensation ageing effect during natural condition, an accelerated UV weathering test was employed to analyze the coating resistance according to ISO 11507 standard test method. The water contact angle, roll-off angle, ice-adhesion strength, percent ice accumulation, and the mechanical performances were measured after the UV weathering test. Comparison with the ones before the UV weathering test is shown in Table 3. It was reported that when a superhydrophobic surface begin to degrade, the water roll-off angle would change more rapidly than the water contact angle. It can be seen that the effect of 288 h's UV and water exposure on the ice-adhesion strength, ice accumulation and mechanical properties of S200 coatings is insignificant, indicating good water condensation and UV resistance. A slight degradation was observed for the S20 coatings. However, the degradation on the PU coatings was more severe than both S20 and S200 coatings.

The micro-sand blaster was used to investigate the erosion resistance of the coatings. Mixture of dry air and abrasive particles in micrometer size was propelled out of a nozzle tip at a high velocity, resulting in an abrasive stream onto the coating surface. Resistance of the tested coatings is determined by the weight loss. Tested samples were weighed before and after 30 s of the sand erosion to an accuracy of ± 0.001 mg. The result is displayed in Figure 5a. A marked

14

lower weight loss was observed for the S200 and PU coatings than S20 coatings, indicating their better erosion resistance. The good sand erosion property of PU coatings is due to its ductile properties, and S200 coatings exhibit comparable sand erosion resistance to commercial PU coatings. To further investigate the erosion damage on the S200 and S20 coatings, FESEM were used to observe the eroded regions on the surface as shown in Figure 5b-c. In the sand-eroded region, micro cutting and ploughing of the relatively soft sol-gel matrix have resulted in the exposure of the harder SiO_2 particles. The damaged surface of the S200 coating presented less porosity than the S20 coating.

The sand erosion also changed the surface morphology of coatings as shown in FESEM images of Figure 5b-c. Large protrusion surface features were observed on the S20 coating surface due to the removal of the porous structure; no air-trap site can be observed (inset in Figure 5b), which explains the decrease in water contact angle and inability to roll off (Table 4). In comparison, the S200 coating (Figure 5c) still maintained some cavity structure after the erosion that enables some degree of air trapping. As a result, the roll-off angle did not increase as much as the one for the S20 coating, and a 10µl water droplet could still roll off though at a much higher angle (Table 4). The PU coating surface was initially relatively smooth with a lower hardness. During the sand erosion test, micro-cutting and ploughing actions removed the coating material and increased the surface roughness. Thus, the PU coating exhibited an increased water contact angle, but the water droplet still could not roll off from the surface due to its high surface energy.

To study the anti-icing durability of coatings, the ice adhesion and the ice accumulation test were carried out after sand erosion. Figure 6 compares the (a) ice-adhesion strength and (b) percentage ice accumulation of the PU, S20 and S200 coatings before and after sand erosion.

15

The ice-adhesion strength and percentage ice accumulation increased substantially after the sand erosion due to the change of surface morphology as discussed before. The induced surface morphology change caused surface wettability change, which has led to the observed degradation in the icephobic performance. Nevertheless, S200 coatings still exhibited better anti-icing properties among others. The adhesion strength remained lower than 100 kPa, implying it possesses excellent anti-icing properties even after the top surface layer is removed since the low surface energy chemicals are still present.[23, 63]

The durability assessment of the S200 coating is summarized in Table S1 (Supplementary Materials) together with other reported coatings in the literature. Caution should be made not to compare some of the performances based on the presented data, since there is a lack of consistent test conditions / standards for the abrasion and erosion tests. Most of the reported icephobic coatings can maintain superhydrophobicity after sandpaper scratching under pressure 2~20 kPa,[13, 64-68] or free-fall sand erosion. However, no ice-adhesion strength or other anti-icing tests were reported. Koivuluoto et al. found weight gain of the polymer coatings after sand erosion at pressure of 2.5 bars (= 250 kPa) but they did report other properties.[69] In comparison, the S200 coatings presented water repellency and icephobicity after sand erosion at pressure of 200 kPa, indicating a very good sand erosion resistance. Some researchers also investigated UV resistance of coatings according to ISO or ASTM standard methods with different irradiation durations.[58, 68, 70-73] With exception of the ice releasing coatings reported by Tang et al.[58], which reported ice-adhesion strength of coatings after UV resistance test, other works only reported the water wettability of coatings. In this study, the ice-adhesion strength of the S200 coating after 144h UV irradiation and 144h water condensation displayed a

~10% increase (to 71.3 kPa), but this strength is lower than the ice-adhesion strength of the topcoat ice-releasing agent reported by Tang et al. before UV exposure (~100 kPa).

So far, the reported superhydrophobic coatings are mainly relied on the loosely bonded and porous structures. Although they can display high water contact angles and low water roll-off angles, most of them are limited in practical applicability due to their poor mechanical properties or durability. Here, we have described a simple method to fabricate durable icephobic coatings by designing the "bulk" coating properties with surface morphology control. The use of silicone-epoxy hybrid resin improves adhesion strength between coatings and the substrates. The resulted coating is room-temperature processable and possesses a water repellent matrix because of the presence of silicone. The addition of PDMS coated dual-sized NPs enables controllable formation of the micro-nanostructured surface, which is mechanically robust yet keeps enough air pockets on the surface. The use of the dual-sized NPs provides the benefits of denser packing while not losing its ability to trap air, and thus is able to maintain excellent water repellence. Such design principle is easy to adopt, scalable, and applicable to other functional coatings. In particular, the extensive mechanical test, UV irradiation with water condensation, and sand erosion test have verified the robustness and durability of the dual-particle S200 coating that has exhibited ice-adhesion strengths below the well-accepted 100 kPa icephobicity criterion.

4. Conclusion

In summary, we have prepared fluorine-free icephobic coatings using a facile and scalable process. A comprehensive investigation has been carried out on the environmental and mechanical durability of the room-temperature processable coatings. The anti-icing and

17

mechanical properties of superhydrophobic coatings with different surface morphology but the same surface chemical structure were analysed. The design of dual-sized NPs has led to better anti-icing properties as well as better resistance to sand erosion and UV weathering than coating with single-sized NPs due to the more favourable surface features. In particular, the ice-adhesion strength of the dual-size SiO_2 NPs coating was lower than 100 kPa after the UV weathering and sand erosion. The developed icephobic coating can be applied for practical applications on outdoor facilities under a harsh working environment.

FIGURES

Figure 1. (a) Schematic drawing of the surface feature formation mechanisms of S20 and S200, and surface morphology of (b) S20 and (c) S200 coatings measured by FESEM. Insets are profile

of 5 µl water droplet on the coating surfaces, scale bar, 1 mm. (d) Measured water contact angles and water roll-off angles of S20 and S200 coatings, (e) surface roughness of S20 and S200 coatings.
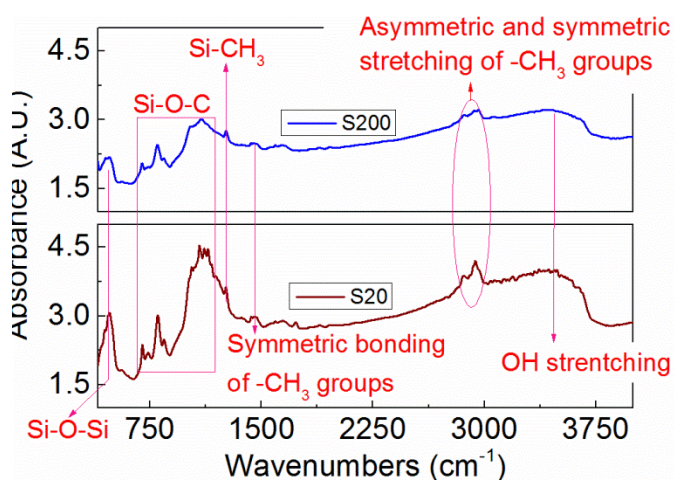

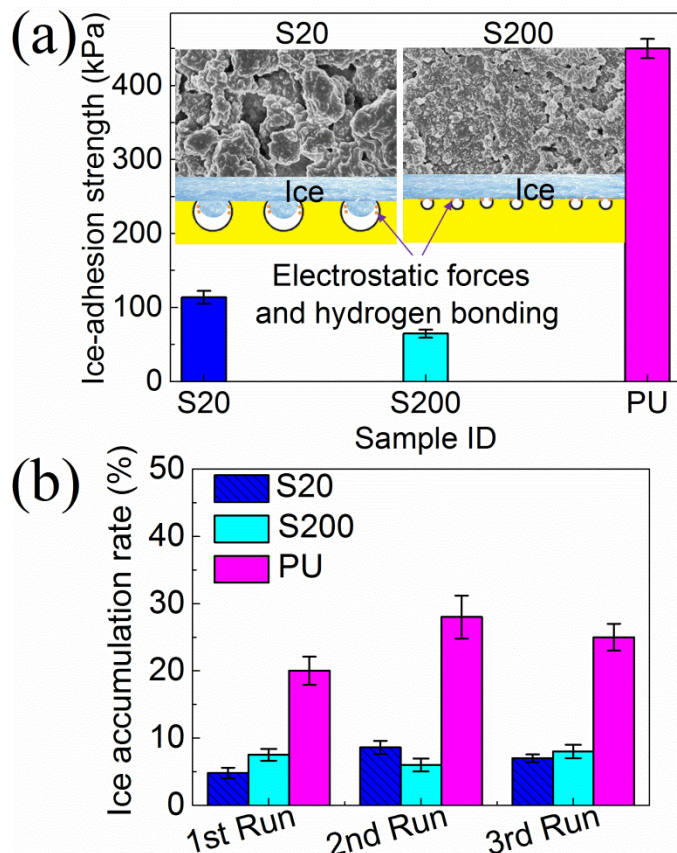**Figure 2.** FTIR spectra of S20 and S200 coating surfaces.

Figure 3. (a) Ice-adhesion strength of S20 and S200 coatings, insets are schematics of ice formation mechanisms on these coating surfaces, (b) ice accumulation results of S20 and S200 coatings.
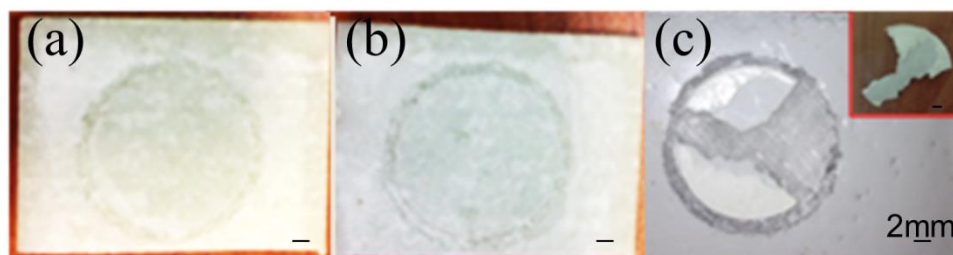

Figure 4. The surface appearance of (a) S20, (b) S200, and (c) PU coatings after the dolly pull-off test, the inset is a large piece peeled-off piece from the PU coating.
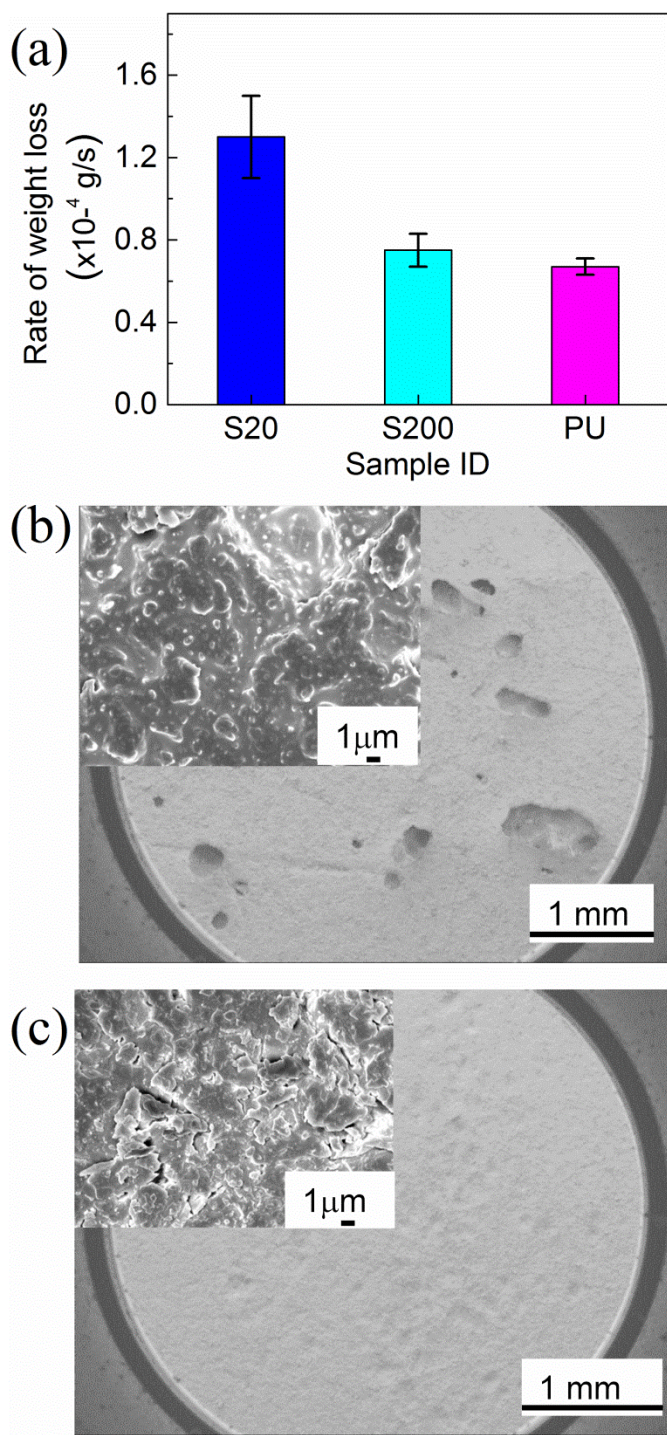
Figure 5. (a) Weight loss of PU, S20 and S200 coatings after sand erosion. FESEM images of (b) S20 and (c) S200 coatings surfaces after sand erosion. Insets in (b) and (c) are the corresponding FESEM images under high magnification.
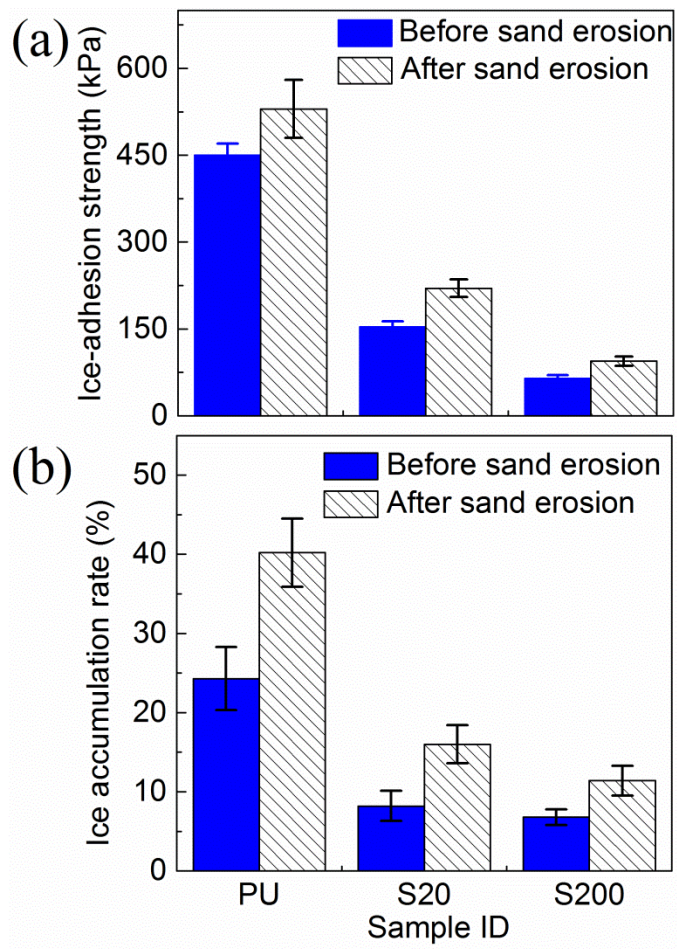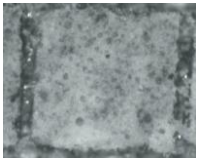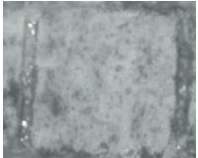
Figure 6. (a) Ice-adhesion strength and (b) ice accumulation of PU, S20 and S200 coatings before and after sand erosion.

TABLES.

Table 1. Sample ID and the corresponding weight ratio of the two types of coatings with different SiO_2 NP sizes.

	SILIKOPON® EF		Sylgard 184		Butyl acetate	SiO_2 NPs		Tinuvin 292
	Part A	Part B	Part A	Part B		200 nm	10-20 nm	
S20	9	4.5	1	0.1	20	0	4	0.08
S200	9	4.5	1	0.1	20	2.67	1.33	0.08

Table 2. Summary of measured mechanical properties of the PU, S20, S200 coatings in comparison with literature data for icephobic coatings.

Testing method	Cross-cut test (ISO 2409)	Pencil scratch test (ISO 15184)	Dolly pull-off test (ISO 4624)* (MPa)	Nano-indentation modulus (GPa)	Nano-indentation hardness (MPa)
PU coating	4B (5 % delaminated areas due to scratch)	4B	5.99 ± 0.16 (B, 45%)*	0.11 ± 0.01	21 ± 3
S20	5B (Nearly no delaminated areas)	3H	> 3.50 ± 0.75 (Y)*	1.28 ± 0.30	37 ± 8
S200	5B (Nearly no delaminated areas)	4H	> 3.70 ± 0.52 (Y)*	2.39 ± 0.66	69 ± 14
Hybrid copolymer film[54]	0B	4B	N/A	N/A	N/A
Icephobic hierarchically textured coatings[55]	5B	N/A	N/A	N/A	N/A
Icephobic superhydrophobic coating[56]	5B	N/A	N/A	N/A	N/A
Al_2O_3 / PTFE icephobic coatings[57]	5B	N/A	N/A	N/A	N/A

Ice Release Coatings[58]		5B	2H~3H	N/A	N/A	N/A
Icephobic paint[59]		N/A	2H	N/A	N/A	N/A
Aeronautical livery coating[60]		5B	N/A	2.41 ± 0.04	4.8 ± 0.3	141 ± 9
Silicone elastomer coating[61]	Without silane-based intermedia layer	N/A	N/A	0.431	N/A	N/A
	With silane-based intermedia layer	N/A	N/A	1.494	N/A	N/A
Bilayer icephobic film via iCVD[62]		N/A	N/A	N/A	19.1 ± 1.2	479 ± 7

* For the PU coating, 45% area of the coating is pulled off from the substrate. Following the test standard, "B" denotes adhesion failure between the coating and the substrate. While for S20 and S200 coatings, due to the low adhesion between the applied adhesive and the superhydrophobic surfaces, the coating did not pull off at the coating/substrate interface. In this case, "Y" indicates failure caused by the applied adhesive. The indicated values are the adhesion strength between the applied adhesive and the coating surface, and the actual coating adhesion strength should be greater than the listed values.

Table 3. Summary of results of coatings properties before and after UV and condensation weathering test.

	PU		S20		S200	
	Before weathering	After weathering	Before weathering	After weathering	Before weathering	After weathering
Water contact angle (°)	98 ± 1.3	83 ± 5.4	157 ± 1.2	154 ± 3.6	158 ± 1.8	156 ± 3.7
Water roll-off angle (°)	No	No	10 ± 1.4	30 ± 2.0	15 ± 2.1	20 ± 1.8
Ice adhesion (kPa)	450.0 ± 13.0	474.0 ± 20.0	113.9 ± 8.8	120.1 ± 9.1	64.7 ± 5.4	71.3 ± 6.8
Ice accumulation (wt. %)	24.3 ± 4.0	30.1 ± 4.3	8.2 ± 1.9	13.0 ± 1.7	6.8 ± 1.0	8.8 ± 1.6
Tape adhesion	4B	4B	5B	5B	5B	5B
Pencil scratch	4B	3H	3H	3H	4H	4H
Dolly pull adhesion (MPa)	5.99 ± 0.16 (B, 45%)	3.81 ± 0.12 (Y)	>3.50 ± 0.75 (Y)	>3.35 ± 0.76 (Y)	>3.70 ± 0.52 (Y)	>3.64 ± 0.65 (Y)
Nano-indentation modulus (GPa)	0.11 ± 0.01	0.12 ± 0.01	1.28 ± 0.30	1.72 ± 0.43	2.39 ± 0.66	2.35 ± 0.68
Nano-indentation hardness (MPa)	21 ± 3	23 ± 3	37 ± 8	76 ± 12	69 ± 14	82 ± 16

Table 4. Water wettability of coatings before and after the sand erosion test.

	PU		S20		S200	
	Before	After	Before	After	Before	After
Water contact angle (°)	98 ± 1.3	103 ± 2.1	157 ± 1.2	132 ± 2.2	158 ± 1.8	148 ± 1.5
Water roll-off angle (°)	No	No	10 ± 1.4	No	15 ± 2.1	85 ± 2.1

Author information

Corresponding Author

* Zhong Chen (aszchen@ntu.edu.sg)

Present Addresses

School of Materials Science and Engineering, Nanyang Technological University, 50 Nanyang Avenue, 639798, Singapore

Author Contributions

Zhong Chen designed this work and guided Xinghua Wu to organize and write this manuscript. Zhao Xin took FESEM images of coatings after sand erosion. Jeffery Weng Chye Ho helped with some mechanical property test.

References

[1] C.A. Lewis, inventor; Adams & Elting Company, assignee. Antifreezing compound. United States patent US 1,282,249. (1918).
[2] C.J. Rolle, W.D. Barnes, Cellulose lacquers-de-icing lacquer for stationary aircraft, Industrial & Engineering Chemistry 48 (1956) 1326-1327.
[3] H. Jellinek, Ice adhesion, Canadian Journal of Physics 40 (1962) 1294-1309.
[4] W. Bascom, R. Cottington, C. Singleterry, Ice adhesion to hydrophilic and hydrophobic surfaces, Journal of Adhesion 1 (1969) 246-263.
[5] J.R. Saroyan, Coatings and encapsulants—preservers in the sea, Ocean Engineering 1 (1969) 435-456.
[6] R.J. Anderson, R.C. Miller, J.L. Kassner Jr, D.E. Hagen, A study of homogeneous condensation-freezing nucleation of small water droplets in an expansion cloud chamber, Journal of the Atmospheric Sciences 37 (1980) 2508-2520.

[7] J.M. Sayward, Seeking low ice adhesion, DTIC Document, 1979.

[8] H.Y. Erbil, A.L. Demirel, Y. Avcı, O. Mert, Transformation of a simple plastic into a superhydrophobic surface, Science 299 (2003) 1377-1380.

[9] A. Lafuma, D. Quéré, Superhydrophobic states, Nature Materials 2 (2003) 457-460.

[10] L. Zheng, Z. Li, S. Bourdo, K.R. Khedir, M.P. Asar, C.C. Ryerson, A.S. Biris, Exceptional superhydrophobicity and low velocity impact icephobicity of acetone-functionalized carbon nanotube films, Langmuir 27 (2011) 9936-9943.

[11] S. Dierer, R. Oechslin, R. Cattin, Wind turbines in icing conditions: performance and prediction, Advances in Science and Research 6 (2011) 245-250.

[12] M. Nosonovsky, V. Hejazi, Why superhydrophobic surfaces are not always icephobic, ACS Nano 6 (2012) 8488-8491.

[13] N. Wang, D. Xiong, S. Pan, K. Wang, Y. Shi, Y. Deng, Robust superhydrophobic coating and the anti-icing properties of its lubricants-infused-composite surface under condensing condition, New Journal of Chemistry 41 (2017) 1846-1853.

[14] Q. Liu, Y. Yang, M. Huang, Y. Zhou, Y. Liu, X. Liang, Durability of a lubricant-infused Electrospray Silicon Rubber surface as an anti-icing coating, Applied Surface Science 346 (2015) 68-76.

[15] J. Zhang, C. Gu, J. Tu, Robust Slippery Coating with Superior Corrosion Resistance and Anti-Icing Performance for AZ31B Mg Alloy Protection, ACS Applied Materials & Interfaces 9 (2017) 11247-11257.

[16] D. Gao, inventor; University of Pittsburgh, assignee. Compositions for prevention of ice build-up. United States patent US 9,688,894. (2017).

[17] Y.H. Yeong, A. Milionis, E. Loth, J. Sokhey, Self-lubricating icephobic elastomer coating (SLIC) for ultralow ice adhesion with enhanced durability, Cold Regions Science and Technology (2018).

[18] M.J. Coady, M. Wood, G.Q. Wallace, K.E. Nielsen, A.-M. Kietzig, F. Lagugné-Labarthet, P.J. Ragogna, Icephobic behavior of UV-cured polymer networks incorporated into slippery lubricant-infused porous surfaces: Improving SLIPS durability, ACS Applied Materials & Interfaces 10 (2018) 2890-2896.

[19] J.H. Li, R. Weng, X.Q. Di, Z.W. Yao, Gradient and weather resistant hybrid super-hydrophobic coating based on fluorinated epoxy resin, Journal of Applied Polymer Science 131 (2014).

[20] A.M. Atta, H.A. Al-Lohedan, A.O. Ezzat, S.A. Al-Hussain, Characterization of superhydrophobic epoxy coatings embedded by modified calcium carbonate nanoparticles, Progress in Organic Coatings 101 (2016) 577-586.

[21] T. Cheng, R. He, Q. Zhang, X. Zhan, F. Chen, Magnetic particle-based super-hydrophobic coatings with excellent anti-icing and thermoresponsive deicing performance, Journal of Materials Chemistry A 3 (2015) 21637-21646.

[22] Y. Si, Z. Guo, W. Liu, A robust epoxy resins@ stearic acid-Mg $(OH)_2$ micronanosheet superhydrophobic omnipotent protective coating for real-life applications, ACS Applied Materials & Interfaces 8 (2016) 16511-16520.

[23] A.M. Emelyanenko, L.B. Boinovich, A.A. Bezdomnikov, E.V. Chulkova, K.A. Emelyanenko, Reinforced superhydrophobic coating on silicone rubber for longstanding anti-icing performance in severe conditions, ACS Applied Materials & Interfaces 9 (2017) 24210-24219.

[24] L. Shen, P. Lu, S. Wang, Z. Chen, Creep behaviour of eutectic SnBi alloy and its constituent phases using nanoindentation technique, Journal of Alloys and Compounds 574 (2013) 98-103.

[25] D. Kumar, X. Wu, Q. Fu, J.W.C. Ho, P.D. Kanhere, L. Li, Z. Chen, Hydrophobic sol–gel coatings based on polydimethylsiloxane for self-cleaning applications, Materials & Design 86 (2015) 855-862.

[26] Q. Fu, D.K. Xinghua Wu, Jeffrey WC Ho, Pushkar D. Kanhere, Narasimalu Srikanth, Erjia Liu, Peter Wilson, and Zhong Chen, Development of sol–gel icephobic coatings: effect of surface roughness and surface energy, ACS Applied Materials & Interfaces 6 (2014) 20685-20692.

[27] X. Wu, S. Zheng, D.A. Bellido-Aguilar, V.V. Silberschmidt, Z. Chen, Transparent icephobic coatings using bio-based epoxy resin, Materials & Design 140 (2018) 516-523.

[28] X. Wu, Q. Fu, D. Kumar, J.W.C. Ho, P. Kanhere, H. Zhou, Z. Chen, Mechanically robust superhydrophobic and superoleophobic coatings derived by sol–gel method, Materials & Design 89 (2016) 1302-1309.

[29] D. Ebert, B. Bhushan, Transparent, superhydrophobic, and wear-resistant coatings on glass and polymer substrates using SiO_2, ZnO, and ITO nanoparticles, Langmuir 28 (2012) 11391-11399.

[30] B.J. Sparks, E.F. Hoff, L. Xiong, J.T. Goetz, D.L. Patton, Superhydrophobic hybrid inorganic–organic thiol-ene surfaces fabricated via spray-deposition and photopolymerization, ACS Applied Materials & Interfaces 5 (2013) 1811-1817.

[31] T.J. Athauda, W. Williams, K.P. Roberts, R.R. Ozer, On the surface roughness and hydrophobicity of dual-size double-layer silica nanoparticles, Journal of Materials Science 48 (2013) 6115-6120.

[32] C. Xue, S. Jia, J. Zhang, L. Tian, H. Chen, M. Wang, Preparation of superhydrophobic surfaces on cotton textiles, Science and Technology of Sdvanced Materials 9 (2008) 035008.

[33] H.J. Tsai, Y.L. Lee, Facile method to fabricate raspberry-like particulate films for superhydrophobic surfaces, Langmuir 23 (2007) 12687-12692.

[34] C.C. Carcouët, A. Esteves, M.M. Hendrix, R.A. van Benthem, G. de With, Fine-tuning of superhydrophobicity based on monolayers of well-defined raspberry nanoparticles with variable dual-roughness size and ratio, Advanced Functional Materials 24 (2014) 5745-5752.

[35] L. Boinovich, A. Emelyanenko, Principles of design of superhydrophobic coatings by deposition from dispersions, Langmuir 25 (2009) 2907-2912.

[36] T. Tadano, R. Zhu, Y. Muroga, T. Hoshi, D. Sasaki, T. Hagiwara, T. Sawaguchi, Characteristics of novel transparent poly (methyl methacrylate)/silica nanoparticle hybrid film prepared based on entanglement-agglomeration transition mechanism, Polymer Journal 47 (2015) 311.

[37] R. Ashokkumar, M. Ramaswamy, Phytochemical screening by FTIR spectroscopic analysis of leaf extracts of selected Indian Medicinal plants, Journal of Current Microbiology and Applied Sciences 3 (2014) 395-406.

[38] S.-H. Wang, P.R. Griffiths, Resolution enhancement of diffuse reflectance ir spectra of coals by Fourier self-deconvolution: 1. CH stretching and bending modes, Fuel 64 (1985) 229-236.

[39] R.H. Auerbach, K. Dost, D.C. Jones, G. Davidson, Supercritical fluid extraction and chromatography of non-ionic surfactants combined with FTIR, APCI-MS and FID detection, Analyst 124 (1999) 1501-1505.

[40] K. Kamiya, T. Yoko, K. Tanaka, M. Takeuchi, Thermal evolution of gels derived from CH3Si (OC2H5) 3 by the sol-gel method, Journal of Non-Crystalline Solids 121 (1990) 182-187.

[41] S. Amoriello, A. Bianco, L. Eusebio, P. Gronchi, Evolution of two acid steps sol–gel phases by FTIR, Journal of Sol-gel Science and Technology 58 (2011) 209-217.

[42] M. Heise, G. Martin, Curing mechanism and thermal properties of epoxy-imidazole systems, Macromolecules 22 (1989) 99-104.

[43] N. Poisson, G. Lachenal, H. Sautereau, Near-and mid-infrared spectroscopy studies of an epoxy reactive system, Vibrational Spectroscopy 12 (1996) 237-247.

[44] N.T. Whilton, S.L. Burkett, S. Mann, Hybrid lamellar nanocomposites based on organically functionalized magnesium phyllosilicate clays with interlayer reactivity, Journal of Materials Chemistry 8 (1998) 1927-1932.

[45] R. Menini, M. Farzaneh, Advanced icephobic coatings, Journal of Adhesion Science and Technology 25 (2011) 971-992.

[46] A. Davis, Y.H. Yeong, A. Steele, I.S. Bayer, E. Loth, Superhydrophobic nanocomposite surface topography and ice adhesion, ACS Applied Materials & Interfaces 6 (2014) 9272-9279.

[47] J. Chen, J. Liu, M. He, K. Li, D. Cui, Q. Zhang, X. Zeng, Y. Zhang, J. Wang, Y. Song, Superhydrophobic surfaces cannot reduce ice adhesion, Appllied Physics Letter 101 (2012) 111603.

[48] V. Hejazi, K. Sobolev, M. Nosonovsky, From superhydrophobicity to icephobicity: forces and interaction analysis, Scientific Reports 3 (2013) 2194.

[49] K. Golovin, S.P. Kobaku, D.H. Lee, E.T. DiLoreto, J.M. Mabry, A. Tuteja, Designing durable icephobic surfaces, Science Advances 2 (2016) e1501496.

[50] L. Cao, A.K. Jones, V.K. Sikka, J. Wu, D. Gao, Anti-icing superhydrophobic coatings, Langmuir 25 (2009) 12444-12448.

[51] S. Farhadi, M. Farzaneh, S. Kulinich, Anti-icing performance of superhydrophobic surfaces, Applied Surface Science 257 (2011) 6264-6269.

[52] C. Antonini, M. Innocenti, T. Horn, M. Marengo, A. Amirfazli, Understanding the effect of superhydrophobic coatings on energy reduction in anti-icing systems, Cold Regions Science and Technology 67 (2011) 58-67.

[53] Z. Chen, L.Y. Wu, E. Chwa, O. Tham, Scratch resistance of brittle thin films on compliant substrates, Materials Science and Engineering: A 493 (2008) 292-298.

[54] Y. Huang, M. Hu, S. Yi, X. Liu, H. Li, C. Huang, Y. Luo, Y. Li, Preparation and characterization of silica/fluorinated acrylate copolymers hybrid films and the investigation of their icephobicity, Thin Solid Films 520 (2012) 5644-5651.

[55] G. Momen, M. Farzaneh, Facile approach in the development of icephobic hierarchically textured coatings as corrosion barrier, Applied Surface Science 299 (2014) 41-46.

[56] R. Menini, Z. Ghalmi, M. Farzaneh, Highly resistant icephobic coatings on aluminum alloys, Cold Regions Science and Technology 65 (2011) 65-69.

[57] R. Menini, M. Farzaneh, Elaboration of Al_2O_3/PTFE icephobic coatings for protecting aluminum surfaces, Surface and Coatings Technology 203 (2009) 1941-1946.

[58] G. Tang, Y.H. Yeong, M. Khudiakov, Ice Release Coatings of High Durability for Aerospace Applications, (2017) 1-17.

[59] S. Kimura, Y. Yamagishi, A. Sakabe, T. Adachi, M. Shimanuki, A new surface coating for prevention of icing on airfoils, SAE Technical Paper, 2007.

[60] L. Mazzola, Aeronautical livery coating with icephobic property, Surface Engineering 32 (2016) 733-744.

[61] M. Esfandeh, S. Mirabedini, S. Pazokifard, M. Tari, Study of silicone coating adhesion to an epoxy undercoat using silane compounds: Effect of silane type and application method, Colloids and Surfaces A: Physicochemical and Engineering Aspects 302 (2007) 11-16.

[62] H. Sojoudi, G.H. McKinley, K.K. Gleason, Linker-free grafting of fluorinated polymeric cross-linked network bilayers for durable reduction of ice adhesion, Materials Horizons 2 (2015) 91-99.

[63] N. Li, L. Wu, C. Yu, H. Dai, T. Wang, Z. Dong, L. Jiang, Ballistic Jumping Drops on Superhydrophobic Surfaces via Electrostatic Manipulation, Advanced Materials (2018).

[64] J. Chen, R. Dou, D. Cui, Q. Zhang, Y. Zhang, F. Xu, X. Zhou, J. Wang, Y. Song, L. Jiang, Robust prototypical anti-icing coatings with a self-lubricating liquid water layer between ice and substrate, ACS Applied Materials & Interfaces 5 (2013) 4026-4030.

[65] Y. Zhang, D. Ge, S. Yang, Spray-coating of superhydrophobic aluminum alloys with enhanced mechanical robustness, Journal of Colloid and Interface Science 423 (2014) 101-107.

[66] Q. Zhang, B. Jin, B. Wang, Y. Fu, X. Zhan, F. Chen, Fabrication of a Highly Stable Superhydrophobic Surface with Dual-Scale Structure and Its Antifrosting Properties, Industrial and Engineering Chemistry Research 56 (2017) 2754-2763.

[67] D. Nanda, P. Varshney, M. Satapathy, S. Mohapatra, B. Bhushan, A. Kumar, Single step method to fabricate durable superliquiphobic coating on aluminum surface with self-cleaning and anti-fogging properties, Journal of Colloid and Interface Science 507 (2017) 397-409.

[68] N. Wang, D. Xiong, Y. Deng, Y. Shi, K. Wang, Mechanically robust superhydrophobic steel surface with anti-icing, UV-durability, and corrosion resistance properties, ACS Applied Materials & Interfaces 7 (2015) 6260-6272.

[69] H. Koivuluoto, C. Stenroos, M. Kylmälahti, M. Apostol, J. Kiilakoski, P. Vuoristo, Anti-icing Behavior of Thermally Sprayed Polymer Coatings, Journal of Thermal Spray Technology 26 (2017) 150-160.

[70] R. Jafari, G. Momen, M. Farzaneh, Durability enhancement of icephobic fluoropolymer film, Journal of Coatings Technology and Research 13 (2016) 405-412.

[71] S. Farhadi, M. Farzaneh, S. Simard, On stability and ice-releasing performance of nanostructured fluoro-alkylsilane-based superhydrophobic Al alloy2024 surfaces, Journal ISSN 1929 (2012) 1248.

[72] L.F. Mobarakeh, R. Jafari, M. Farzaneh, Robust icephobic, and anticorrosive plasma polymer coating, Cold Regions Science and Technology (2018).

[73] F. Wang, S. Yu, J. Ou, W. Li, Anti-icing performance of transparent and superhydrophobic surface under wind action, Journal of Sol-Gel Science and Technology 75 (2015) 625-634.